Integrated Modeling of CO_2 Storage and Leakage Scenarios Including Transitions between Super- and Sub-Critical Conditions, and Phase Change between Liquid and Gaseous CO_2

Karsten Pruess

Earth Sciences Division, Lawrence Berkeley National Laboratory
University of California, Berkeley, CA 94720, USA
K_Pruess@lbl.gov

ABSTRACT

Storage of CO_2 in saline aquifers is intended to be at supercritical pressure and temperature conditions, but CO_2 leaking from a geologic storage reservoir and migrating towards the land surface (through faults, fractures, or improperly abandoned wells) would reach sub-critical conditions at depths shallower than 500-750 m. At these and shallower depths, subcritical CO_2 can form two-phase mixtures of liquid and gaseous CO_2, with significant latent heat effects during boiling and condensation. Additional strongly non-isothermal effects can arise from decompression of gas-like subcritical CO_2, the so-called Joule-Thomson effect. Integrated modeling of CO_2 storage and leakage requires the ability to model non-isothermal flows of brine and CO_2 at conditions that range from supercritical to subcritical, including three-phase flow of aqueous phase, and both liquid and gaseous CO_2. In this paper we describe and demonstrate comprehensive simulation capabilities that can cope with all possible phase conditions in brine-CO_2 systems. Our model formulation includes

- an accurate description of thermophysical properties of aqueous and CO_2-rich phases as functions of temperature, pressure, salinity and CO_2 content, including the mutual dissolution of CO_2 and H_2O;
- transitions between super- and sub-critical conditions, including phase change between liquid and gaseous CO_2;
- one-, two-, and three-phase flow of brine-CO_2 mixtures, including heat flow;

- non-isothermal effects associated with phase change, mutual dissolution of CO_2 and water, and (de-) compression effects;
- effects of dissolved NaCl, and the possibility of precipitating solid halite, with associated porosity and permeability change.

Applications to specific leakage scenarios demonstrate that the peculiar thermophysical properties of CO_2 provide a potential for positive as well as negative feedbacks on leakage rates, with a combination of self-enhancing and self-limiting effects. Lower viscosity and density of CO_2 as compared to aqueous fluids provides a potential for self-enhancing effects during leakage, while strong cooling effects from liquid CO_2 boiling into gas, and from expansion of gas rising towards the land surface, act to self-limit discharges. Strong interference between fluid phases under three-phase conditions (aqueous - liquid CO_2 - gaseous CO_2) also tends to reduce CO_2 fluxes. Feedbacks on different space and time scales can induce non-monotonic behavior of CO_2 flow rates.

1. Introduction

CO_2 storage reservoirs as currently envisioned will place CO_2 at depths greater than 800 m, where CO_2 is in supercritical conditions, with both pressure and temperature exceeding the critical values of P_{crit} = 73.82 bar, T_{crit} = 31.04 ^{o}C.[1] However, subcritical conditions involving both liquid and gaseous CO_2 may evolve if CO_2 escapes from the primary storage reservoir, and migrates upward through improperly abandoned wells or faults and fractures to conditions of lower temperatures and pressures.[2-7] Such migration would give rise to three-phase flow involving an aqueous phase (native brine), liquid CO_2, and gaseous CO_2, with strong non-isothermal effects from phase change and decompression of CO_2.[3, 4, 8, 9] A rigorous assessment of the potential impacts associated with leakage of CO_2 from deep storage reservoirs must be based on an accurate representation of the underlying physical and chemical processes that determine the multiphase flow and heat transfer behavior of CO_2 in geologic media.[10-14]

This paper describes and demonstrates numerical techniques that can seamlessly model CO_2 storage and leakage processes from the deep subsurface all the way to the land surface, including transitions between super- and sub-critical conditions, boiling of liquid CO_2 into gas,

and associated multi-phase, non-isothermal flow processes. These simulation capabilities are implemented in a new fluid property module called "ECO2M" that operates within the general TOUGH2-framework for modeling non-isothermal multiphase flows in porous and fractured media.[15] TOUGH2/ECO2M considers all possible phase combinations in the brine-CO_2 system as well as transitions between them, including the precipitation and dissolution of solid salt (halite). Below, we begin by highlighting the rich phase-change behavior during upward migration of CO_2 from geologic storage sites. We then discuss the challenges of selecting primary thermodynamic variables for the various phase conditions and transitions in brine-CO_2 mixtures, and we subsequently apply the new TOUGH2/ECO2M code to explore CO_2 storage and leakage scenarios.

2. Phase Transitions in the CO_2-Brine System During Upward Migration

Figs. 1-2 show typical temperature and pressure conditions in terrestrial crust, corresponding to a geothermal gradient of 30 ^oC/km and fresh water in hydrostatic pressure equilibrium, relative to land surface conditions of (T, P) = (15 ^oC, 1.013 bar). It is seen that temperature and pressure conditions will pass near the critical point of CO_2 at depths of 500 - 750 m. CO_2 storage in saline aquifers will be at supercritical conditions, where CO_2 forms a single phase that is immiscible with water, and has liquid-like density and gas-like viscosity. When both temperature and pressure are below the critical values, i.e., for CO_2 migrating upwards from a deep geologic storage site, CO_2 may exist in two different phase states, liquid or gas, as well as in liquid-gas two-phase mixtures. The seven possible phase combinations for brine-CO_2 mixtures are shown in Fig. 3; the number of phase combinations doubles to fourteen when allowing for the possibility of solid salt appearing and disappearing. These multiphase mixtures and their associated non-isothermal transitions strongly control CO_2 and brine transport processes (e.g., fluid flow, mass transport, and heat transfer), while at the same time presenting difficult challenges for quantitative analysis and modeling, due to non-linear feedbacks between different processes and parameters. Below we discuss numerical methods that permit rigorous flow and transport simulation for conditions ranging from the deep subsurface to shallow near-surface environments, thereby enabling integrated modeling of CO_2 storage and leakage.

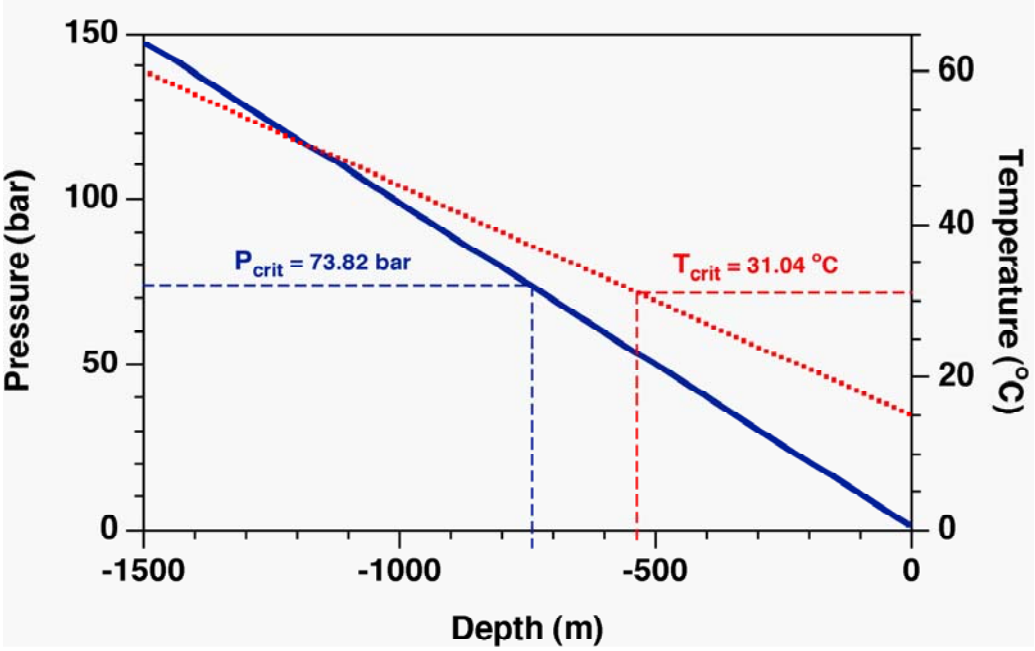

Figure 1. Typical temperature and pressure profiles in terrestrial crust.

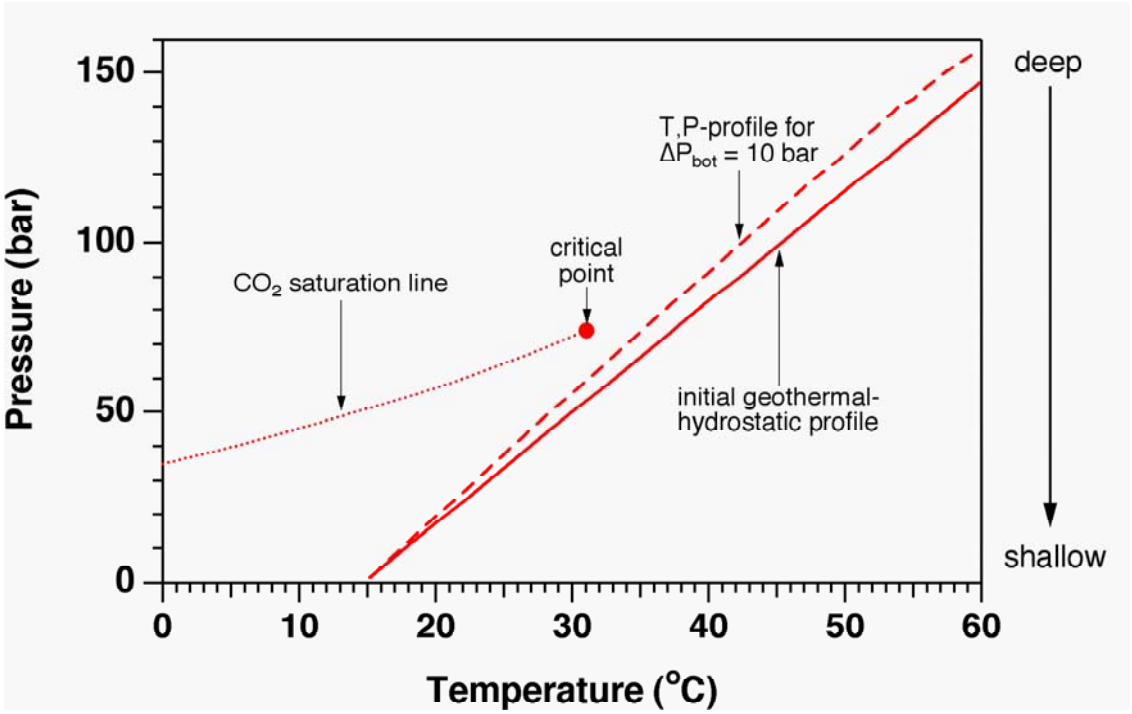

Figure 2. T,P-diagram of a typical geothermal-hydrostatic profile. The CO_2 saturation line is also shown, as is a profile that corresponds to a pressure increase of $\Delta P = 10$ bar at 1500 m depth.

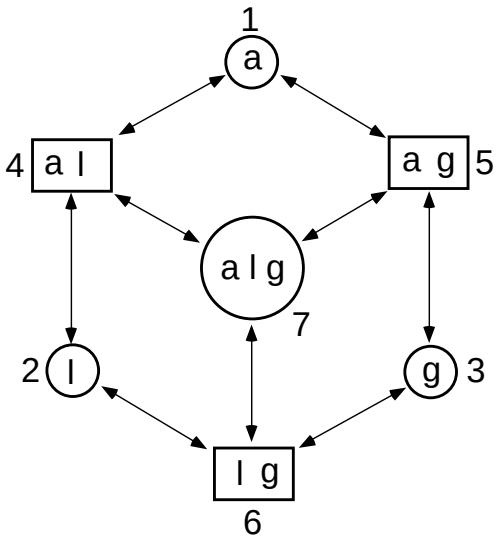

Figure 3. Possible phase combinations in the system brine-CO_2. The phase designations are a - aqueous, l - liquid CO_2, g - gaseous CO_2. Separate liquid and gas phases exist only at subcritical conditions.

3. Numerical Methods

3.1 Thermophysical Properties and Primary Thermodynamic Variables

Fundamental to any calculation of flow and transport in complex systems is the definition of primary variables, which are the essential variables that describe the (local) thermodynamic state of the system, and whose change with time is determined by the underlying mass-and-energy balance equations.[15] The methods for choosing primary variables for integrated modeling of CO_2 storage and leakage scenarios are embedded in ECO2M, an extension of the ECO2N fluid property module for TOUGH2.[10] ECO2M uses the same correlations as ECO2N to describe thermodynamic and thermophysical properties of H_2O–NaCl–CO_2 mixtures largely within experimental errors for temperatures in the range 10 $^oC \leq T \leq 110$ ^oC, pressures $P \leq 600$ bar, and salinity up to full halite saturation. Essential properties include density, viscosity, and specific enthalpy of fluid phases as function of temperature, pressure, and composition; and partitioning of mass components H_2O, NaCl and CO_2 among the different phases. Depending upon the phase combination present, not all thermodynamic parameters are independent; for example, when both a liquid and gaseous CO_2-rich phase are present, pressure is a unique function of temperature. This issue is addressed by using different sets of primary thermodynamic variables for different phase combinations (see Table 1), and "switching" primary variables when phases appear or

disappear. The meaning of variables not yet explained is X - mass fraction of CO_2, S_a - saturation of aqueous phase, S_g - saturation of gas phase, and Y - mass fraction of water. The second primary variable X_{sm} refers to NaCl and denotes salt mass fraction X_s in the two-component water-salt system when there is no solid salt, or "solid saturation" $X_{sm} = S_s+10$ when halite precipitate is present. Here, "solid saturation" S_s denotes the fraction of pore volume with solid salt. The reason for adding a number 10 to the second primary variable when solid salt is present is to change the numerical range to the interval (10, 11), and to thus be able to distinguish

Table 1. Primary thermodynamic variables used for multiphase mixtures of brine and CO_2.

Phase Conditions	Phase Index*	Primary Variables			
		1	2	3	4
aqueous only	1	P	X_{sm}	X	T
liquid only	2	P	X_{sm}	X	T
gas only	3	P	X_{sm}	X	T
aqueous and liquid	4	P	X_{sm}	S_a	T
aqueous and gas	5	P	X_{sm}	S_a	T
liquid and gas	6	P	X_{sm}	S_g	Y
three phase	7	P	X_{sm}	S_a	S_g

* see Fig. 3.

conditions with and without solid salt simply by the numerical range of the second primary variable. In ECO2N as in most other fluid property packages for the TOUGH2 simulator, different phase compositions are identified by means of different numerical ranges of the primary variables, an approach that works well when only a few different phase compositions need to be distinguished. This technique is retained in ECO2M for treating the appearance and disappearance of a solid halite phase. However, such an approach would become awkward for

the seven different fluid phase compositions considered in ECO2M. Accordingly, ECO2M uses a different approach, in which different phase compositions, and the meaning of primary thermodynamic variables, are identified and distinguished by means of a numerical index, that ranges from 1 to 7 as shown in Fig. 3 and Table 1. In addition to facilitating the identification of phase compositions and recognition of primary thermodynamic variables, using an index to identify phase conditions offers the possibility to "decouple" the assignment of phase conditions from the numerical values of primary variables. As will be seen below, this provides flexibility in the handling of phase transitions (appearance and disappearance of phases), which can be exploited to greatly improve the stability and robustness of the numerical solution.

3.2 Phase Change

When thermodynamic conditions change in the course of a simulation, the primary thermodynamic variables are monitored to determine whether phase conditions change. For example, for a grid block in single-phase aqueous conditions, we need to monitor CO_2 content to determine whether a (liquid or gaseous) CO_2-rich phase evolves. A transition to two-phase conditions will occur if dissolved CO_2-mass fraction X exceeds the equilibrium solubility $X_{aq,l}$ at prevailing conditions of pressure, temperature, and salinity. If $X > X_{aq,l}$ a liquid CO_2-rich phase evolves, the phase index is changed to #4 (see Table 1), and the new phase is initialized with a small saturation $S_l \approx 10^{-6}$ by setting the third primary variable (aqueous phase saturation) to $S_a = 1 - S_l\ (= 10^{-6}) - S_s$. (If pressure is sub-critical and below saturated vapor pressure of CO_2 at prevailing temperature, the phase transition is not made to aqueous-liquid but is made to aqueous-gas conditions, with phase index #5.) For a grid block that is in two-phase a-l (aqueous-liquid, index = 4) conditions, we monitor the third primary variable, aqueous phase saturation S_a. Liquid phase saturation is $S_l = 1 - S_s - S_a$, so that, as long as $0 < S_a < 1\text{-}S_s$, we have $S_l > 0$ and two-phase a-l conditions are maintained. If $S_a > 1\text{-}S_s$, the liquid CO_2 phase disappears, and we make a transition from a-l to single-phase aqueous conditions. If $S_a \leq 0$, the aqueous phase disappears, and we transition to single-phase liquid conditions. For a-l conditions at sub-critical temperatures, we also need to check whether a gaseous CO_2 phase evolves. This is done by comparing fluid pressure with the CO_2 saturation pressure at prevailing temperature, $P_{sat,CO2}(T)$. Ignoring the effects of water on fluid pressures, which are small at the modest temperatures considered here, we require $P \geq P_{sat,CO2}$ in order that no gas phase evolves. If this inequality is

violated, we make a transition to three-phase a-l-g conditions, and initialize the new gas phase with a small saturation of order 10^{-6}. Fig. 3 indicates that there are 18 possible phase changes between the 7 possible phase combinations, and similar checks and initialization procedures are employed for all of them.

According to the previous discussion, phases appear or disappear whenever primary variables change past certain "sharp" threshold values. Experience with modeling CO_2 leakage scenarios has shown that such "hairtrigger" criteria for phase change may be prone to generating unstable behavior, with severe limitations for attainable time steps, especially when dealing with transitions between a <==> a-l <==> a-l-g <==> a-g. We achieve a more robust behavior by introducing a "finite window" for phase change, as follows. In the first of the above examples, instead of performing a transition from a ==> a-l conditions whenever $X > X_{aq,l}$, we evolve a liquid CO_2 phase only when dissolved CO_2 mass fraction X exceeds the equilibrium solubility $X_{aq,l}$ by a finite amount, $X > (1+\delta)X_{aq,l}$. Here, δ is a small parameter of order 10^{-3} - 10^{-5}. Similarly, instead of making the transition a-l ==> a-l-g whenever $P < P_{sat,CO2}$, we evolve a gas phase only when P drops below $P_{sat,CO2}$ by a finite amount, $P < (1-\delta)P_{sat,CO2}$. As a further refinement, we may optionally apply a "hairtrigger" criterion for phase change for the first few Newtonian iterations during a time step, and switch to a finite window for the subsequent Newtonian iterations. We have found that dynamic finite-size windows for phase change are essential for robust and efficient simulation of highly non-linear flow processes that involve boiling and condensation of liquid and gaseous CO_2 phases, with strong associated latent heat effects.

From a thermodynamic standpoint, it is possible for liquid CO_2 to change into gas, or vice versa, without any phase change, as long as the path from initial to final state avoids crossing the CO_2 saturation line. In order to achieve a consistent description of CO_2 phase conditions throughout the entire T,P-plane, we adopt the convention that, for supercritical temperatures, a change between liquid and gaseous CO_2 conditions is made whenever fluid pressure moves past the critical value. Note that this change of phase designation is merely an accounting device, and fluid properties for $T > T_{crit}$ vary continuously when P changes past P_{crit}.

Strong non-isothermal effects may occur when CO_2 escapes from the primary storage reservoir and migrates upwards along localized preferential pathways, such as faults and fracture zones, or improperly abandoned wells.[3, 6, 9] For such scenarios, the fate and transport of CO_2 may be strongly affected by heat transfer between the CO_2 flow path(s) and surrounding media of low permeability. As will be seen below, feedbacks between fluid flow and heat transfer can occur on a broad range of time scales, placing a premium on the accurate representation of heat transfer effects. Our numerical approach uses the semi-analytical method of Vinsome and Westerveld[16] to accurately represent heat transfer between fluids in a permeable fault zone and the adjacent wall rocks over a broad range of space and time scales, without any need to explicitly include the wall rocks in the simulation domain.[4] In the next section, we apply the new methods built into TOUGH2/ECO2M to relevant CO_2 leakage problems. Note that although our numerical methods can treat (NaCl) brines up to full halite saturation, all scenarios investigated here assume the aqueous phase to be fresh water.

4. CO_2 Discharge from a Deep Fault Zone

We consider a highly idealized problem of CO_2 leakage from a deep storage reservoir along a single vertical fault zone of 5 m thickness. The fault is assumed to intersect the CO_2 reservoir at a depth of Z = -1500 m. Fault zone permeability is assumed as $k = 100 \times 10^{-15}$ m^2, porosity $\phi = 15$ %, with wall rocks assumed completely impermeable. Initial conditions in the fault correspond to hydrostatic equilibrium of fresh (non-saline) water in a typical geothermal gradient, as shown in Figs. 1-2. Running a single-phase aqueous system with land surface conditions of $(T_0, P_0) = (15\ ^oC, 1.013 \times 10^5\ Pa)$ in a geothermal gradient of 30 ^oC/km to hydrostatic equilibrium, initial conditions at Z = -1500 m depth are found to be (T, P) = (60 ^oC, 147.475 bar). Despite the relative simplicity of the leakage scenario considered here, we show below that highly complex phase changes occur that create complicated flow processes, demanding a thorough treatment of phase combination possibilities as provided in TOUGH2/ECO2M.

The present scenario does not model the CO_2 storage reservoir as such; instead, we assume that a CO_2 plume from a storage reservoir reaches the bottom of the fault zone at some pressure in excess of hydrostatic. We model a finite-length section of the fault as a 1-D system,

and initiate upflow of CO_2 by specifying boundary conditions of supercritical CO_2 at an overpressure of 10 bar relative to hydrostatic pressure at the bottom of the fault. Land surface conditions are kept unchanged. The pressurization from the step change in bottom boundary conditions rapidly migrates up the fault; the resulting T, P-profile is shown in Fig. 2. In response to CO_2 injection water is being pushed upward, and a front of free-phase CO_2 is advancing towards the land surface. Little is presently known about the relative permeability behavior of three-phase mixtures of aqueous and liquid and gaseous CO_2-rich phases. For the simulations we use the same relative permeability formulation due to Stone[17] as had been employed in our previous analysis of a secondary CO_2 accumulation scenario,[9] treating liquid CO_2 as intermediately wetting between the (wetting) aqueous and (non-wetting) gas phases. Our model accounts for non-isothermal effects that arise from (1) upflow of warmer (T = 60 ^oC) fluid into colder regions, (2) Joule-Thomson cooling as upflowing CO_2 expands,[18, 19] (3) boiling of liquid CO_2 into gas, and (4) mutual dissolution of H_2O and CO_2.

An important aspect of system evolution is conductive heat exchange with the wall rocks, which we model by means of a semi-analytical method.[16] As originally conceived by Vinsome and Westerveld[16] and used in standard TOUGH2, the semi-analytical approach for modeling conductive heat exchange was designed for confining beds with low permeability, such as cap rocks and base rocks. In that case the boundary of the permeable region typically occurs at a fixed vertical depth, and the initial temperature T_i at the boundary of the conduction zone is approximately the same for all grid blocks that have an interface with the conduction zone. For such applications, the entire conduction zone may be considered to have the same initial temperature. The situation may be quite different in CO_2 leakage, where the pathways are more likely to be (sub-)vertical, and the initial temperature distribution along the leakage path would be given by a geothermal gradient. To be able to cope with such conditions, TOUGH2/ECO2M offers the possibility of modeling temperature gradients along the boundary to the conduction zone by specifying the initial temperature of the conductive half-spaces to be different for different grid blocks.

The CO_2 entering the fault displaces some of the aqueous phase, dissolves a small amount of water, and also partially dissolves into the aqueous phase. Most CO_2 remains in a

separate liquid-like phase that is advancing towards the land surface. The liquid CO_2 starts boiling at about 530 m depth, giving rise to significant temperature decline. Additional (Joule-Thomson) cooling occurs at shallower depths, as gaseous CO_2 expands. The cooling effects induce conductive heat transfer from the wall rocks. The flow system evolves a three-phase zone, with strong interference between the aqueous and liquid and gaseous CO_2-rich phases reducing fluid mobility. This reduces CO_2 upflow rates, which over time allows temperatures to recover by conductive heat transfer from the wall rocks. Liquid then boils away, reducing phase interference and causing CO_2 flow rates to again increase. The interplay between fluid flow and heat transfer gives rise to quasi-periodic cycling of CO_2 fluxes and extent of three-phase conditions (Figs. 4-6).

Our simulation stops after 36.3 yr (1.145×10^9 s), when temperatures near 275 m depth approach the freezing point of water. Fig. 4 shows profiles of temperature and CO_2 phase saturations at different times. The saturation profile at t = 6.42 yr gives a snapshot just prior to commencement of CO_2 discharge at the land surface at 6.425 yr. Note a sharp transition from liquid to gaseous CO_2 at 530 m depth. As will be seen below (Fig. 7), this transition occurs almost exactly at the critical point of CO_2. Over time the system experiences predominant cooling effects, and evolves an extended region with 3-phase fluid conditions (aqueous - liquid CO_2 - gaseous CO_2). After t = 27.13 yr, three-phase conditions are seen to extend from - 240 m to -460 m depth (note that an aqueous phase is present throughout, the profile of which at t = 27.13 yr is also shown in Fig. 4). There is a precipitous temperature decline in the three-phase zone, reflecting heat loss as liquid CO_2 boils into gas. Lowest temperatures are reached at the liquid CO_2 front, where rates of boiling and associated heat loss are largest. We note that saturations of liquid CO_2 increase to large values beneath the three-phase zone. This represents buoyant accumulation of liquid CO_2 beneath a region of low effective fluid mobility. The three-phase zone acts as a mobility block, because in three-phase conditions, relative permeabilities are small for all phases. Within the three-phase zone, liquid and gas saturations show strong fluctuations, which are due to a subtle interplay between multiphase flow and conductive heat transfer across the fault walls with different time constants. Aqueous phase saturation $S_{aq} = 1 - (S_{liq}+S_{gas})$ shows much smaller fluctuations than either S_{liq} or S_{gas}.

At early times, outflow at the land surface is just aqueous phase. A large "burp" of water outflow occurs as free CO_2 approaches the land surface, reflecting the strong volume expansion there (Fig. 5). CO_2 flux at the land surface shows non-monotonic behavior. Periods of large CO_2 outflow correlate with declining temperatures of the discharge (Fig. 5). The largest CO_2 flux approaches $2x10^{-3}$ kg/s/m^2, which for the assumed fault zone thickness of 5 m translates into an outflow rate of somewhat less than 10^{-2} kg/s per meter fault length, or 1 kg/s per 100 m fault length. During periods when the CO_2 outflow rate is relatively small, three-phase conditions migrate upward, and the region with three-phase conditions thickens (Fig. 6). As CO_2 outflow rates increase, the upward extension of three-phase conditions slows and eventually turns around when liquid CO_2 is boiled off the top of the three-phase zone at large rates.

Additional insight into the system dynamics can be gained by examining the evolution of profiles in T,P-space. Fig. 7 shows that, as a consequence of the pressure increase and temperature decline during CO_2 migration, the T,P-profile is rapidly shifted towards the CO_2 saturation line. Thermodynamic conditions get drawn towards the critical point and then approximately follow the saturation line. Note that three-phase points must fall right on the saturation line, while in the vicinity of three-phase zones, thermodynamic conditions will plot near the saturation line. At time t = 27.13 yr we have a large extent of three-phase conditions (Figs. 4, 6), and a correspondingly large region of T,P-conditions overlapping with the saturation line. Temperatures have a local minimum at the lowest pressure (shallowest depth) with three-phase conditions. Temperatures increase near the bottom of the overlying two-phase aqueous-gas zone, but resume enhanced decline from Joule-Thomson cooling as the upflowing gas expands upon its approach to the land surface.

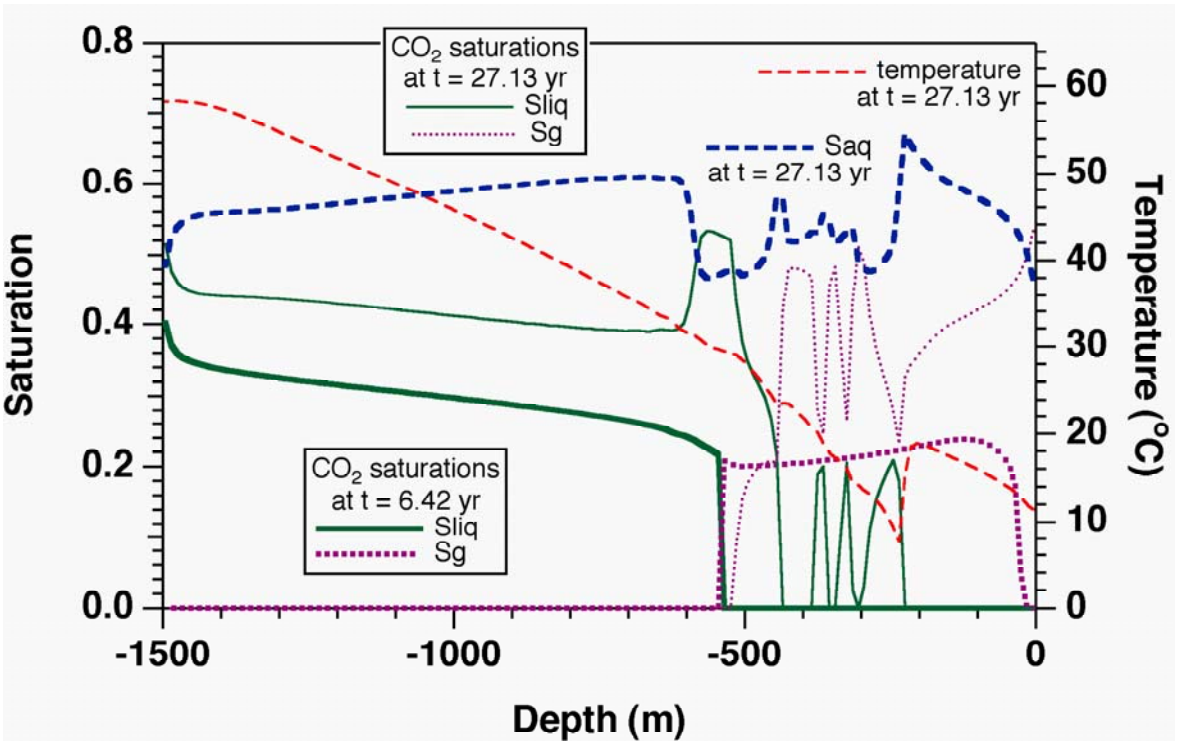

Figure 4. Saturation and temperature profiles at different times.

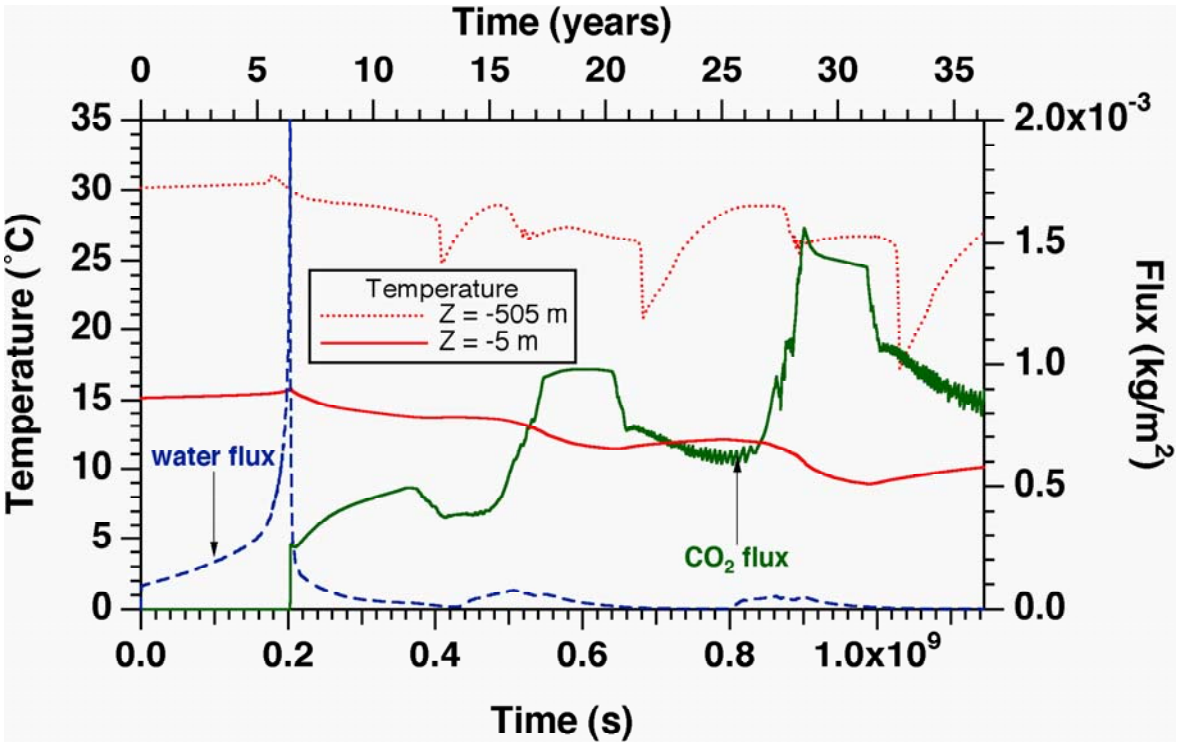

Figure 5. Time dependence of water and CO_2 outflow at the landsurface, and temperatures at two different depths.

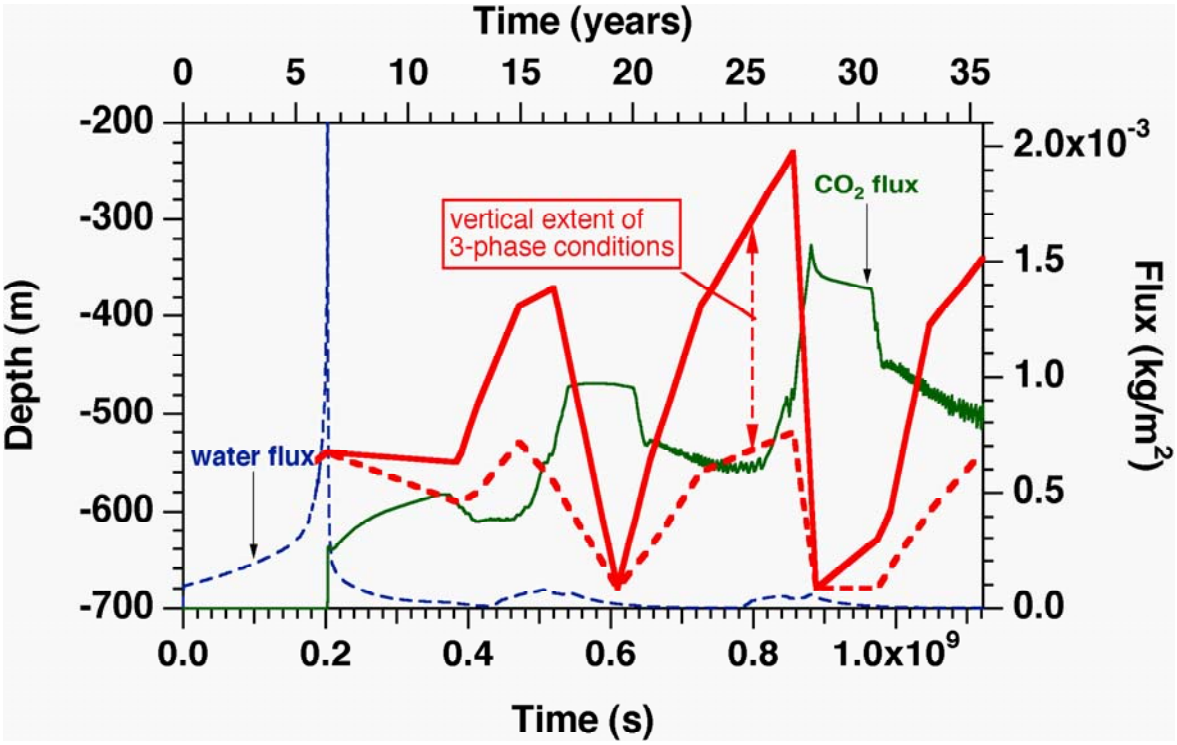

Figure 6. Water and CO_2 fluxes as shown in Fig. 5, with the heavy superposed lines indicating the top and bottom of three-phase conditions, respectively.

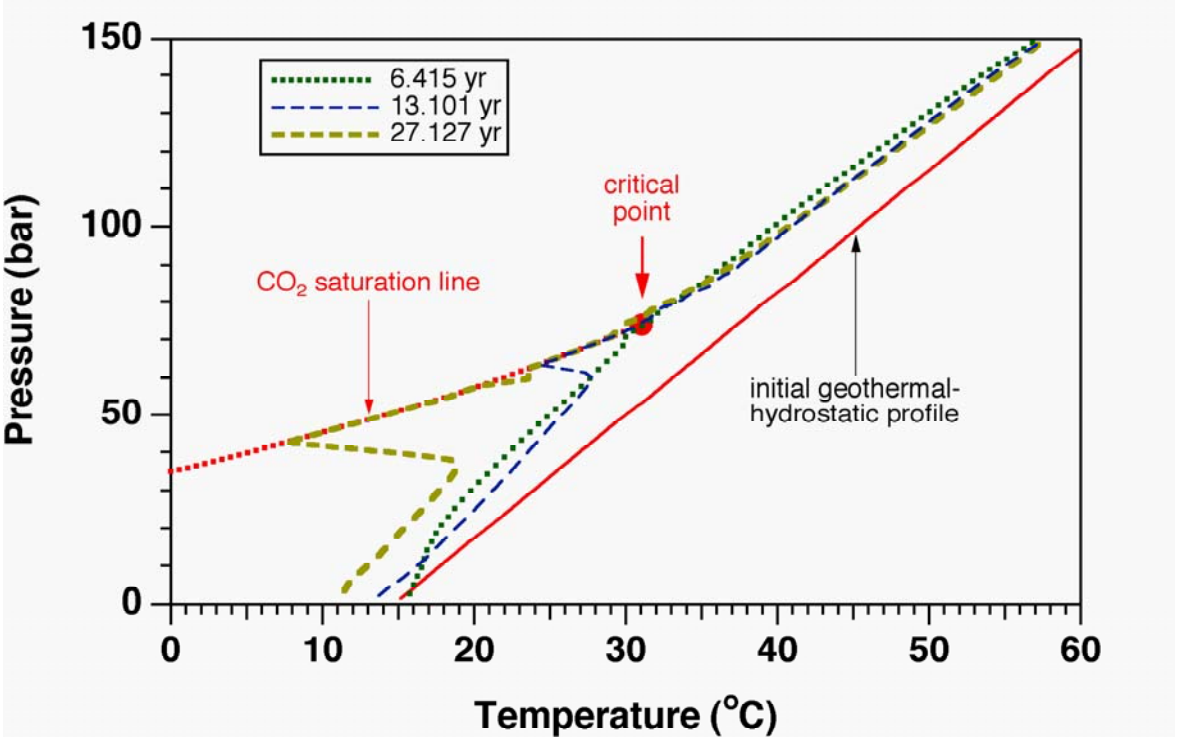

Figure 7. Temperature-pressure profiles at different times.

5. Migration of a CO_2 Plume in a Sloping Aquifer, Intersected by a Fault

This problem explores a scenario that includes the primary CO_2 storage reservoir, as well as a leakage pathway that extends all the way to the land surface. We consider the large-scale long-time migration of a CO_2 plume in a sloping aquifer that is intersected by a leaky fault. Aquifer parameters are patterned after the Carrizo-Wilcox aquifer at the Texas Gulf coast;[20, 21] no effects of salinity are presently included. We assume that a substantial number of CO_2 storage projects will be operating in the Wilcox, and we consider a 2-D vertical section along the dip of the aquifer. The aquifer is modeled as a rectangular domain of 200 m thickness and 110 km length, sandwiched between impermeable cap and base rocks, and tilted with an angle of $\alpha = 1.5^o$ against the horizontal (Fig. 8). We consider the upper right hand corner of the domain to be at the land surface; the lower left hand corner is then at a depth of $110{,}000 \sin(\alpha) + 200 \cos(\alpha)$, which for a tilt angle of $\alpha = 1.5^o$ corresponds to 3,079.4 m. Formation properties include a uniform and isotropic permeability of 500 mD, a porosity of 15 %, and a compressibility of 4.5×10^{-10} Pa^{-1} (similar to compressibility of water at ambient conditions). The 2-D computational grid for the aquifer models a section of 1 m thickness; it has 7300 blocks with a basic space discretization of

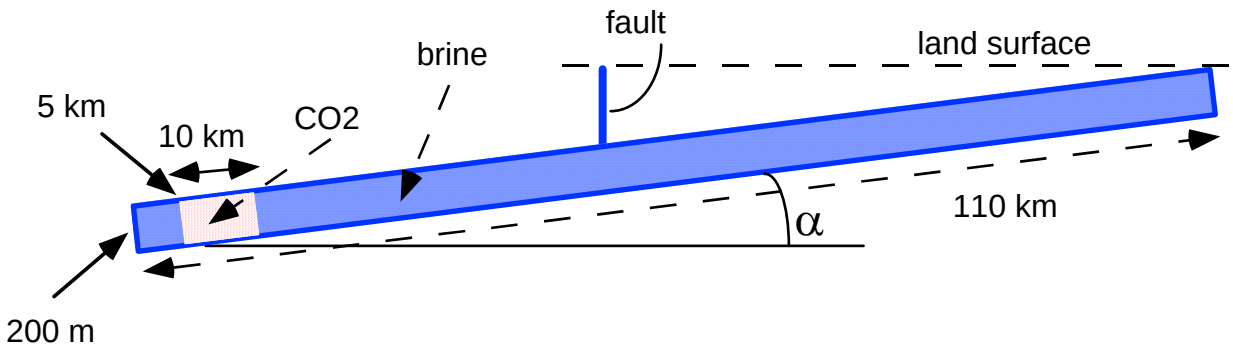

Figure 8. Geometric dimensions of the 2-D rectangular domain modeled (not to scale). The domain is dipping upward by an angle α. The initial CO_2 plume is shown by light shading.

10 m in the sub-vertical and 1000 m in the sub-horizontal direction. The grid was refined to ΔZ = 1 m near the top, to better resolve the CO_2 plume, and to ΔY = 10 m in the Y-direction near Y = 50 km where a vertical fault intersects the aquifer at a depth of 1570.75 m. The fault zone has a thickness of 10 m. Vertical discretization in the fault is also ΔZ = 10 m, hydrogeologic properties are assumed identical to those in the aquifer, and land surface conditions of (T_0, P_0) = (10 ^{o}C,

1.013×10^5 Pa) are maintained at the top of the fault. Boundary conditions for the aquifer are "no flow" everywhere, except for the fault connection and at the upper right hand corner, which is held at land surface conditions. The flow system is initialized as a fully (fresh-) water-saturated medium in hydrostatic equilibrium, held in a geothermal gradient of grad(T) = 30 ^{o}C/km relative to a land surface temperature of 10 ^{o}C.

Our interest in this problem is in the long-term migration of stored CO_2. For long-term CO_2 behavior the actual time dependence of CO_2 injection is not important, and is not modeled here. Instead, the CO_2 plume is emplaced instantaneously by assigning a uniform gas saturation of S_g = 80 % to the subdomain labeled "CO2" in Fig. 8, corresponding to aqueous phase at irreducible saturation of $S_{aq,ir}$ = 20 %; for the CO_2 emplacement, pressures and temperatures are kept unchanged at their initial values, which for the center of the plume are (P, T) = (265 bar, 91.5 ^{o}C). Plume evolution takes place under the combined action of gravity and pressure forces, with CO_2 buoyancy due to lower density being the primary driving force. As in the previous fault upflow problem, conductive heat exchange across the fault walls is an important part of the evolution of the system, and is again modeled with the semi-analytical technique of Vinsome and Westerveld;[16] conductive heat exchange between the aquifer and cap and base rocks is less significant, but is included as well.

A detailed discussion of the plume migration problem without a leaky fault present has been given elsewhere.[22] Here we primarily highlight features of the simulation that pertain to the role of the leaky fault. The simulation is run for a total of 10,000 time steps. CO_2 reaches the fault after a simulation time of 186.5 yr and 855 time steps, but simulation time advances only another 126.0 yr during the subsequent 9,145 time steps. The much smaller time steps after CO_2 reaches the fault are due to the highly dynamic processes in the fault, including CO_2 boiling and condensation, two- and three-phase flow, and conductive heat transfer with the wallrocks. Water flux at the bottom of the fault is small and positive (= upward) at early times, turning negative (downward) after CO_2 enters the fault at t = 186.5 yr (Figs. 9, 10). The onset of CO_2 discharge at the top of the fault at $t = 6.22585 \times 10^9$ s = 197.3 yr is preceded by a large "burp" of water outflow, in response to the strong volume expansion of CO_2 approaching the land surface. Water and CO_2 fluxes subsequently go through cyclic variations, reflecting the interplay of processes

on three different time scales, (1) multiphase flow in the fault, (2) heat exchange with the fault walls, and (3) coupling between fluid pressures and CO_2 upflow rates in the storage aquifer at the bottom of the fault.

Prior to the CO_2 plume reaching the fault, its advancement is virtually identical to a case without a leaky fault, that had been previously simulated using TOUGH2/ECO2N (Fig. 11).[22] After the CO_2 plume reaches the fault its further advancement stalls for a while, but then resumes at an essentially unchanged rate. This behavior is a consequence of the variable plume thickness, see Fig. 12. The tip of the plume is very thin, and total CO_2 flow rate is small near the plume tip, allowing all of the advancing CO_2 to be leaked off when the plume first reaches the fault. At later time thicker portions of the plume approach the fault, total CO_2 flow rate increases, and only a fraction of the CO_2 plume can be captured by the fault. The CO_2 bypassing the fault then resumes its updip migration at the same speed as before the fault intercepted the plume. Fig. 11 also shows that CO_2 loss up the fault is substantial, amounting to almost 7 % of original CO_2 inventory over a 100-year period of fault leakage.

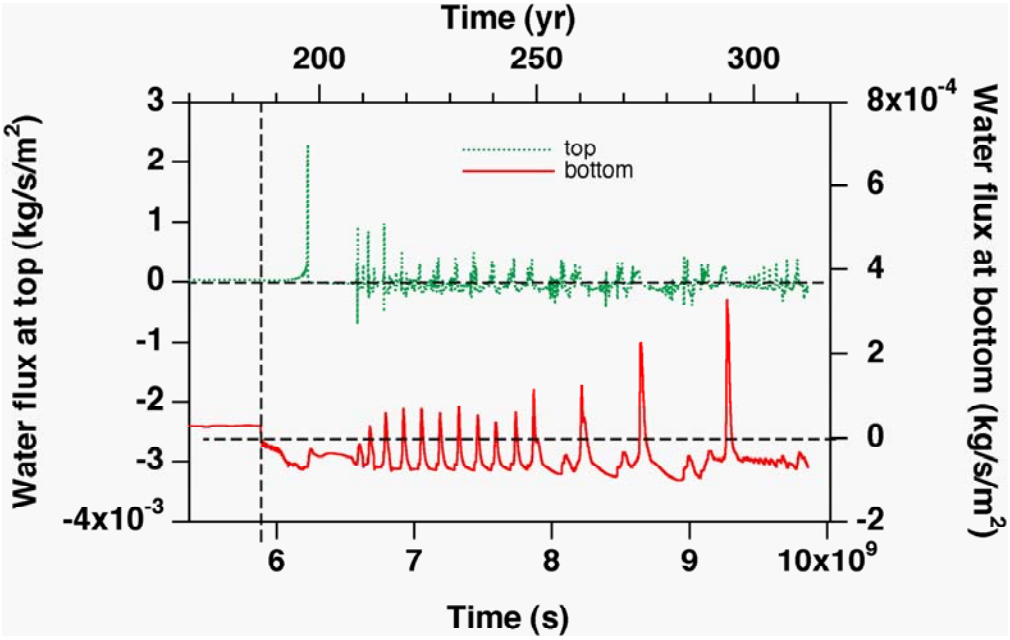

Figure 9. Water fluxes at the top and bottom of the fault. The dashed line at t = 186.5 yr indicates the time at which CO_2 first reaches the fault.

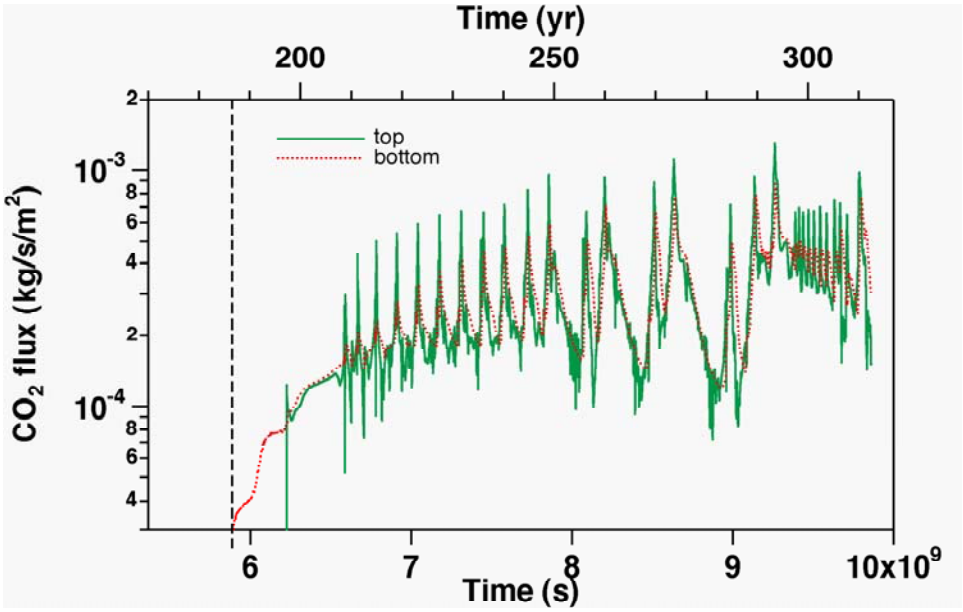

Figure 10. CO_2 fluxes at the top and bottom of the fault. The dashed line at t = 186.5 yr indicates the time at which CO_2 first reaches the fault.

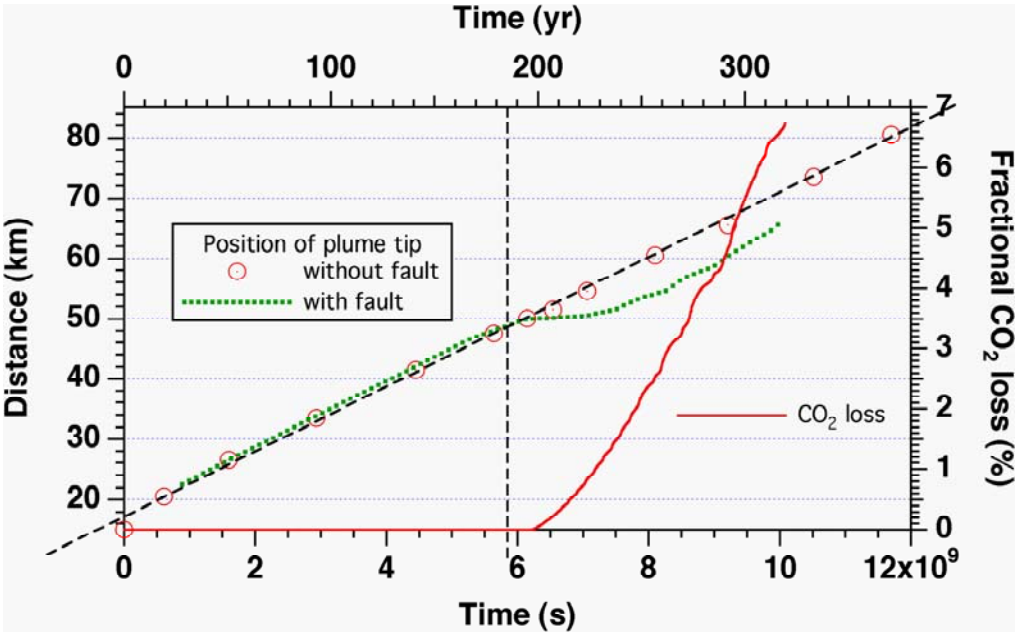

Figure 11. Advancement of the plume over time. The data for the case without a fault are from a TOUGH2/ECO2N simulation,[22] and the dashed straight line is an eye-fit to these data. CO_2 loss by leakage up the fault as fraction of initial inventory is also shown. The dashed vertical line at t = 186.5 yr indicates the time at which CO_2 first reaches the fault.

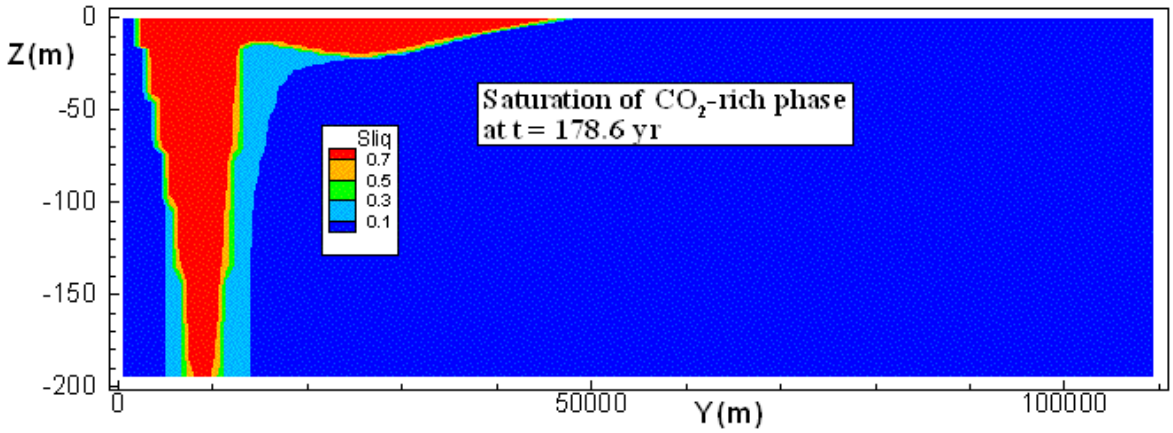

Figure 12. CO_2 plume at t = 178.6 yr, just prior to CO_2 reaching the leaky fault that intersects the reservoir top at Y = 50,000 m.

6. Concluding Remarks

We have developed numerical simulation capabilities for coupled fluid and heat flows that involve all possible phase compositions of brine-CO_2 mixtures, including super- and sub-critical conditions, and three-phase mixtures of aqueous phase, and liquid and gaseous CO_2 phases. This allows seamless modeling of CO_2 storage and leakage in the temperature range 10 $^{o}C \leq T \leq 110\ ^{o}C$, pressures up to 600 bar, and dissolved NaCl with salinity up to full halite saturation. The new modeling capabilities are embodied in a computer code "TOUGH2/ECO2M" that will be made available to the public.

Applications to idealized CO_2 leakage scenarios, with CO_2 migrating from a deep storage reservoir to the land surface through direct preferential pathways, demonstrate a complex interplay of multiphase fluid flow and heat transfer. CO_2 rising towards the land surface may evolve into two-phase mixtures of liquid and gaseous CO_2 as temperatures and pressures decrease, inducing three-phase flow of CO_2-brine mixtures, with strong cooling effects as liquid CO_2 boils into gas, and as gaseous CO_2 expands (Joule-Thomson effect). The emergence of three-phase conditions (aqueous - liquid CO_2 - gaseous CO_2) leads to low mobilities for all phases and acts to reduce CO_2 discharge rates. Strong coupling between multiphase flow and heat transfer on different time scales gives rise to non-linear feedbacks, some of which are self-enhancing while others are self-limiting. Field observations of natural analogues and experimental studies of leakage on a scale approaching actual CO_2 storage systems will be

required to more fully establish the reliability and credibility of these modeling results. The interplay of feedbacks on different time scales can induce non-monotonic flow behavior and a tendency towards cyclic variations of fluid discharges. Such behavior may facilitate monitoring of CO_2 storage systems, as it may provide signals that may be more easily distinguished from background noise.

Future work needs to address issues of relative permeability and capillary pressure behavior of two- and three-phase brine-CO_2 mixtures,[23-25] including hysteretic effects,[26, 27] as well as the coupling of fluid flow and heat transfer to chemical and mechanical interactions between fluids and rocks.[11, 28]

Acknowledgement

Thanks are due to Curt Oldenburg for a careful review of the manuscript and the suggestion of improvements. We also thank anonymous reviewers for constructive suggestions. This work was supported by the Assistant Secretary for Fossil Energy, Office of Coal and Power R&D, through the National Energy Technology Laboratory, and by the Zero Emission Research and Technology project (ZERT) under Contract No. DE-AC02-05CH11231 between the U.S. Department of Energy and the Lawrence Berkeley National Laboratory.

References

1. Vargaftik, N.B. *Tables on the Thermophysical Properties of Liquids and Gases*, 2nd Ed., John Wiley & Sons, New York, NY, 1975.

2. Celia, M.A., S. Bachu, J.M. Nordbotten, S.E. Gasda and H.K. Dahle. Quantitative Estimation of CO_2 Leakage from Geological Storage: Analytical Models, Numerical Models, and Data Needs, paper 18-01, *Proceedings, 7th International Conference on Greenhouse Gas Control Technologies,* Vancouver, Canada, 2004.

3. Pruess, K. Numerical Simulation of CO_2 Leakage from a Geologic Disposal Reservoir, Including Transitions from Super- to Sub-Critical Conditions, and Boiling of Liquid CO_2, *Soc. Pet. Eng. J.,* pp. 237 - 248, June 2004.

4. Pruess, K. Numerical Simulations Show Potential for Strong Non-isothermal Effects During Fluid Leakage from a Geologic Disposal Reservoir for CO_2, B. Faybishenko, P.A. Witherspoon and J. Gale (eds.), *Dynamics of Fluids and Transport in Fractured Rock,*

Geophysical Monograph 162, pp. 81–89, American Geophysical Union, Washington, DC, 2005.

5. Nordbotten, J.M., M.A. Celia, S. Bachu and H.K. Dahle. Semianalytical Solution for CO_2 Leakage through an Abandoned Well, *Environ. Sci. Technol.,* Vol. 39, No. 2, pp 602–611, DOI: 10.1021/es035338i, 2005.

6. Nordbotten, J.M., D. Kavetski, M.A. Celia and S. Bachu. Model for CO_2 Leakage, Including Multiple Geological Layers and Multiple Leaky Wells, *Environ. Sci. Technol.,* Vol. 43, pp. 743–749, 2009.

7. Annunziatellis A., S.E. Beaubien, S. Bigi, G. Ciotoli, M. Coltella and S. Lombardi. Gas migration along fault systems and through the vadose zone in the Latera caldera (central Italy): Implications for CO_2 geological storage, *Int. J. Greenhouse Gas Control,* Vol. 2, Issue 3, pp. 353–372, doi:10.1016/j.ijggc.2008.02.003, 2008.

8. Skinner, L. CO_2 Blowouts: An Emerging Problem, *World Oil,* Vol. 224, No., 1, 2003.

9. Pruess, K. Leakage of CO_2 from Geologic Storage: Role of Secondary Accumulation at Shallow Depth, *Int. J. Greenhouse Gas Control,* Vol. 2, Issue 1, pp. 37–46, doi:10.1016/S1750-5836(07)00095-3, 2008.

10. Pruess K. and N. Spycher. ECO2N – A Fluid Property Module for the TOUGH2 Code for Studies of CO_2 Storage in Saline Aquifers, *Energy Conversion and Management,* Vol. 48, No. 6, pp. 1761–1767, doi:10.1016/j.enconman.2007.01.016, 2007.

11. Gherardi, F., T. Xu and K. Pruess. Numerical Modeling of Self-limiting and Self-enhancing Caprock Alteration Induced by CO_2 Storage in a Depleted Gas Reservoir, *Chem. Geol.,* Vol. 244, pp. 103–129, 2007.

12. Class, H. et al. A Benchmark Study on Problems Related to CO_2 Storage in Geologic Formations, *Comput. Geosci.,* Vol. 13, pp. 409–434, 2009.

13. Kopp, A., P.J. Binning, K. Johannsen, R. Helmig and H. Class. A Contribution to Risk Analysis for Leakage Through Abandoned Wells in Geological CO_2 Storage, *Adv. Wat. Resour.,* Vol. 33, pp. 867–879, 2010.

14. Siirila, E.R., A.K. Navarre-Sitchler, R.M. Maxwell and J.E. McCray. A Quantitative Methodology to Assess the Risks to Human Health from CO_2 Leakage into Groundwater. *Adv Water Resour,* doi:10.1016/j.advwatres.2010.11.005, in press 2011.

15. Pruess, K. The TOUGH Codes—A Family of Simulation Tools for Multiphase Flow and Transport Processes in Permeable Media, *Vadose Zone J.,* Vol. 3, pp. 738 - 746, 2004b.

16. Vinsome, P.K.W. and J. Westerveld. A Simple Method for Predicting Cap and Base Rock Heat Losses in Thermal Reservoir Simulators, *J. Canadian Pet. Tech.*, 19 (3), 87–90, July-September 1980.

17. Stone, H.L. Probability Model for Estimating Three-Phase Relative Permeability, *Trans. SPE of AIME,* 249, 214-218, 1970.

18. Katz, D.L. and R.L. Lee. *Natural Gas Engineering,* McGraw-Hill Publ. Comp., New York, NY 1990.

19. Oldenburg, C.M. Joule-Thomson cooling due to CO_2 injection into natural gas reservoirs, *Energy Conversion and Management*, *48*, 1808-1815, 2007.

20. Nicot, J.-P. Evaluation of Large-Scale CO_2 Storage on Fresh-Water Sections of Aquifers: An Example from the Texas Gulf Coast Basin, *Int. J. Greenhouse Gas Control,* Vol. 2, Issue 4, pp. 583–593, 2008.

21. Hesse, M.A., F.M. Orr, Jr., and H.A. Tchelepi. Gravity Currents with Residual Trapping, *J. Fluid Mech.,* Vol. 611, pp. 35–60, 2008.

22. Pruess, K. and J. Nordbotten. Numerical Simulation Studies of the Long-term Evolution of a CO_2 Plume in a Saline Aquifer with a Sloping Caprock, *Transport in Porous Media,* DOI: 10.1007/s11242-011-9729-6, February 2011.

23. Chiquet, P., J.L. Daridon, D. Broseta and S. Thibeau. CO_2/water Interfacial Tensions under Pressure and Temperature Conditions of CO_2 Geological Storage, *Energy Conv. Managemt.,* Vol. 48, pp. 736–744, 2007.

24. Bachu, S. and B. Bennion. Effects of In-situ Conditions on Relative Permeability Characteristics of CO_2-brine Systems, *Environ. Geol.,* DOI 10.1007/s00254-007-0946-9, 2007.

25. Bachu, S. and D.B. Bennion. Interfacial Tension between CO_2, Freshwater, and Brine in the Range of Pressure from (2 to 27) MPa, Temperature from (20 to 125) °C, and Water Salinity from (0 to 334 000) mg·L-1, *J. Chem. Eng. Data,* Vol. 54, pp. 765–775, 2009.

26. Juanes, R., E.J. Spiteri, F.M. Orr, Jr., and M.J. Blunt. Impact of Relative Permeability Hysteresis on Geological CO_2 Storage, *Water Resour. Res.,* Vol. 42, W12418, doi:10.1029/2005WR004806, 2006.

27. Doughty, C. Modeling Geologic Storage of Carbon Dioxide: Comparison of Non-hysteretic and Hysteretic Characteristic Curves, *Energy Conv. Managmt.,* Vol. 48, pp. 1768–1781, 2007.

28. Rutqvist, J., J. Birkholzer and C.F. Tsang. Coupled Reservoir-geomechanical Analysis of the Potential for Tensile and Shear Failure Associated with CO_2 Injection in Multilayered Reservoir-caprock Systems, *Int. J. Rock Mech. Mining Sci.,* Vol. 45, No. 2, pp. 132–143, February 2008.